Urban Pedestrian Navigation Using Smartphone-Based Dead Reckoning and 3-D Map-Aided GNSS

Li-Ta Hsu, *Member, IEEE*, Yanlei Gu, *Member, IEEE*, Yuyang Huang, and Shunsuke Kamijo, *Member, IEEE*

Abstract—This paper focuses on the pedestrian navigation in highly urbanized area, where a current smartphone and a commercial global navigation satellite system (GNSS) receiver perform poorly because of the reflection and blockage of GNSS signal by buildings and foliage. A 3-D map-aided pedestrian positioning method is previously developed to mitigate and correct the multipath GNSS signal. However, it still suffers from the low availability due to the insufficient number of satellites. We develop a smartphone-based pedestrian dead reckoning (PDR) algorithm, which is carried in the pedestrian's trousers. This PDR is capable of not only providing continues solutions but also indicating the pedestrian motions. A closed-loop Kalman filter with adaptive tuning is proposed to integrate the 3-D map-aided GNSS method with the smartphone-based PDR system. According to the experiment results, the proposed integration system can achieve ~1.5- and 5.5-m of positioning errors in a middle-class and deep urban canyon, respectively.

Index Terms—Pedestrian, dead reckoning, GNSS, GPS, 3-dimensional digital map, smartphone, urban canyon.

I. INTRODUCTION

LOCALIZATION in urban environments becomes essential due to the increasing requirement of navigation service for blind and vision impaired pedestrians. Global navigation satellite system (GNSS) receiver is one of the most popular sensors to navigate the user in a global scale. However, the commercial-grade GNSS receiver performs poorly in the urban area covered by dense buildings. The signal blockage and reflection which is well-known as multipath effect results in more than tens of meters in terms of positioning error [1], [2]. Recently, the use of three-dimension (3D) city building model as an aid to mitigate, exclude or even correct the multipath and non-line-of-sight (NLOS) effects becomes popular in GNSS research field [3]–[12]. In 2013, the research team of The University of Tokyo developed a particle filter based GNSS positioning method using a basic 3D city building to estimate the positioning result of commercial GNSS single frequency receiver [7], [8], [12]. We call it 3D-GNSS. However, the 3D-GNSS method still suffers from the signal blockage in deep urban canyons or the modern foliage tunnel in urban

streets, especially in the scenarios that less than 4 satellites can be received [12]. For the pedestrian, it is important to provide a continuous and accurate navigation system. A sensor integration system is a highly potential candidate to achieve the preferable performance. For the pedestrian navigation, other promising sensors are the MEMS accelerometer, gyroscope and magnetometer sensors embedded in the smartphone and they are usually used together to provide the pedestrian dead reckoning (PDR).

PDR systems have developed using dedicated sensor units mounted on the body, for instance, on a waistband [13]–[15], a shoe [16]–[18], or a helmet [19], [20]. Those approaches make assumption that the IMU is attached to a fix positioning on pedestrian's body. In [21]–[26] and [25]–[33] PDR methods were proposed to use a mobile device that is carried in the pedestrian's trouser pocket or hand, respectively, and therefore, has no fixed orientation. Since most smartphones and other recent mobile devices are equipped with various sensors, PDR can now be deployed to these everyday devices. A review of PDR until 2013 can be found at [34]. The proposed PDR method also uses a mobile device placed freely in the user's trouser front pocket, where people most commonly carry their mobile phones (especially males). In other words, our method does not depend on a priori knowledge of the device's orientation. From the viewpoint of user-acceptable usage, it is not realistic to limit users to keep their phones in a rigidly fixed position and orientation. However, the PDR requires another system to provide absolute position of pedestrian as a starting point. In addition, the proposed smartphone based PDR mainly uses the MEMS magnetometer to estimate the heading direction, which can be easily affected by the surrounding ferrous objects.

The objective of this paper is therefore to integrate the previous developed 3D-GNSS with the proposed smartphone based PDR to provide complimentary support to each other. This paper implements a close-loop Kalman filter to conduct the integration, that the 3D-GNSS and PDR provide the measurement and propagation model, respectively. The reliability of the 3D-GNSS is not consistent in every seconds. Thus, we design a new adaptive measurement noise calibration algorithm for the implemented Kalman filter. In order to show the necessarily of the 3D-GNSS in urban canyon, we also use the GNSS solutions calculated by an open source GNSS software, a smartphone and a commercial-GNSS receiver to integrate with the proposed smartphone-based PDR. The result shows
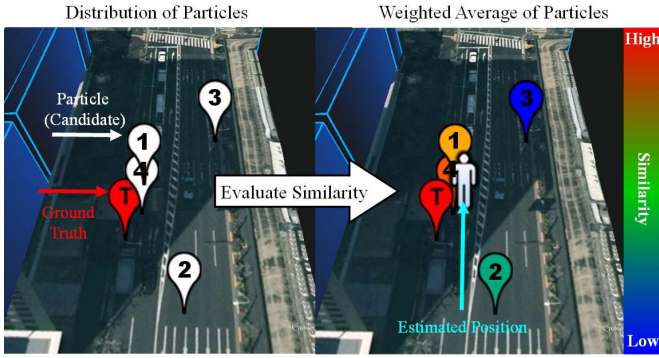
Fig. 1. Demonstration of distribution of particles and final estimated position using the 3D-GNSS method.

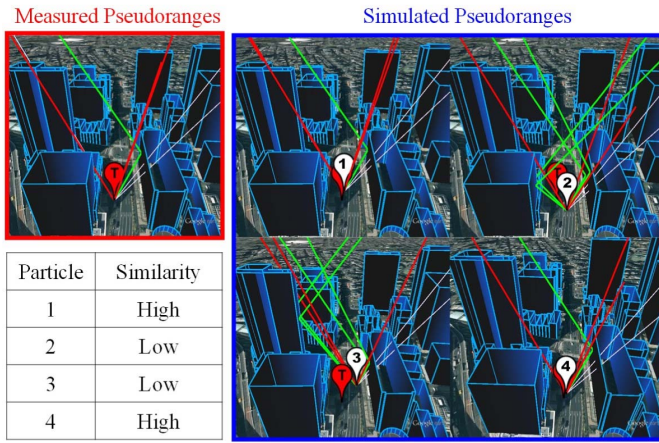| Particle	Similarity
1	High
2	Low
3	Low
4	High

Fig. 2. Calculation of the pseudorange similarity using the measured pseudorange from GNSS receiver and simulated pseudorange by 3D building and ray-tracing.

that the proposed solution, 3D-GNSS+PDR can achieve the best performances among other competitors in deep urban environments.

Accordingly, this paper is organized as follows: A brief introduction and difficulties of the 3D-GNSS method are given in Section 2. Introduction of the proposed smartphone-based PDR is introduced in Section 3. Detail of the integration algorithm between the 3D-GNSS and the PDR is presented in Section 4. The experimental setup and results are shown in Section 5. Finally, the conclusions and future work of this paper are summarized in Section 6.

II. 3D MAPS AIDED GNSS METHOD (3D-GNSS)

A. Methodology of 3D-GNSS

The 3D-GNSS method first distributes the random position candidates as shown in the left Fig. 1, and then calculates the pseudorange similarities between raw pseudo-range measurements and the simulated pseudoranges for each candidate as shown in Fig.2. The simulated pseudorange is calculated with the help of the 3D building models and ray-tracing technique [35]. By comparing the pattern of pseudoranges, the pseudorange similarity can be estimated and
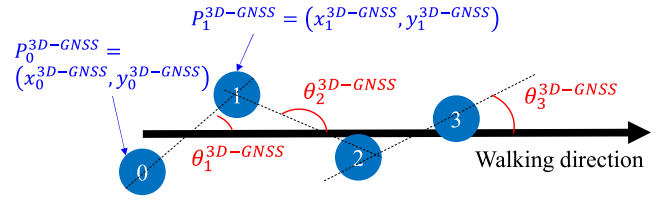

Fig. 3. Illustration of the estimation of heading angle using 3D-GNSS method.

expressed as (1):

$$d_{pr}^{(j)} = \min_{\delta t^{\mathrm{r}}} \sum_{n}^{N^{\mathrm{sim}}} \frac{\left| \rho_n - \hat{\rho}_n^{(j)}\left(\delta t^{\mathrm{r}}\right) \right|}{N^{\mathrm{sim}}} \quad (1)$$

where, $d_{pr}^{(j)}$ denotes the pseudorange similarity for particle j, δt^{r} denotes the receiver clock bias, N^{sim} denotes the number of satellite simulated and ρ_n and $\hat{\rho}_n^{(j)}$ denote the pseudorange measurement and simulated pseudorange, respectively.

The likelihood of each candidate is based on its pseudorange similarity. Finally, the weighted average of the positions of the candidates is regarded as the estimated position result as shown in the right of Fig. 1. This paper assumes the distribution of the pseudorange similarity is fitted to Gaussian function with a standard deviation, σ_0. The equation of the weighted average is listed as below:

$$P^{3D-GNSS} = \frac{\sum_j e^{-\left(d_{pr}^{(j)2}/\sigma_0^2\right)} P^{(j)}}{\sum_i e^{-\left(d_{pr}^{(j)2}/\sigma_0^2\right)}} \quad (2)$$

where $P^{(j)}$ denotes the position of particle j and σ_0 is set to 20 meters empirically. The detail of the 3D-GNSS method can be found in [7] and [8]. The previous developed 3D-GNSS is used to estimate the user position originally. For the purpose of correcting the bias angle of the PDR, this paper extends the usage of the 3D-GNSS to estimate the heading angle as well.

B. Heading Angle Estimated by 3D-GNSS

The basic idea of using 3D-GNSS to estimate pedestrians' heading angle is to assume the pedestrian dynamic does not change dramatically in a short period of time. Thus, we can use a sequence of the estimated positions to calculate the heading angle. The idea is illustrated in Fig.3.

In Fig. 3, a heading angle can be easily estimated using two epochs of the position result, which can be expressed as (3).

$$\theta_i^{3D-GNSS} = bearing\left(P_{i-1}^{3D-GNSS}, P_i^{3D-GNSS}\right), \quad (3)$$

where subscript i denotes the index of epoch and *bearing* represents the calculation of the absolute bearing angle, namely the angle between or true North and an object. However, the variation of the heading angle using only two epochs is too large to be used in the integration. To reduce the variation, we consider several epochs to calculate the heading angle. Besides, if the time of estimated heading angle is closer to the current time, the weighting is higher. The calculation
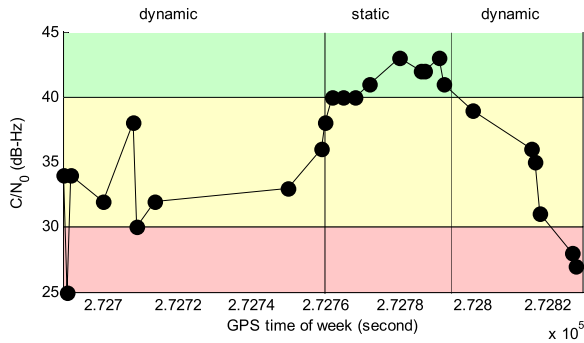
Fig. 4. Illustration of the C/N_0 difference of NLOS to be received in static and dynamic motions.

of the 3D-GNSS estimated heading angle, $\Theta_i^{3D-GNSS}$, is expressed as (4).

$$\Theta_i^{3D-GNSS} = \frac{\sum_{k=0}^{T-1} (T-k) \, \theta_{i-k}^{3D-GNSS}}{\sum_{k=0}^{T-1} (T-k)}, \tag{4}$$

where T denotes the number of epoch used to calculated heading angle and it is set to 5 epochs in this paper.

C. Problem Statement of Using 3D-GNSS

The 3D-GNSS is previously shown effective to provide accurate positioning performance in middle class urban canyons. However, it still suffers from two difficulties. The first is the low availability due to lack of received satellites in deep urban canyon. In the deep urban canyon, the number of received GNSS satellite is usually less than 4 satellite due to the blockage of the buildings and dense foliage. Naturedly, the 3D-GNSS cannot provide a position solution if less than 4 satellites are received. In this case, the PDR is a good candidate to provide system propagation while the unavailability of 3D-GNSS. The second difficulty is the variation of the carrier to noise ratio (C/N_0) of NLOS signal. In the real world, it is ambiguous to determine the type of the received GNSS signals, namely LOS, multipath or NLOS. A popular metric used to classify the signal type is according C/N_0 [36]. However, the C/N_0 of multipath signal to be received in static and dynamic motion could be different. According to [37], the C/N_0 is calculated using a certain length of signal carrier. If the multipath signal is received by dynamic motion, the multipath signal changes dramatically in the certain period which result in low C/N_0 value. On the other hand, in the static scenario, the multipath is continuously to be received, its C/N_0 became stronger. An example of the strong C/N_0 of NLOS in the static data is given as below.

As can be seen from Fig.4, the C/N_0 of NLOS is stronger in static data than it in dynamic data. This stronger C/N_0 makes the receivers to believe it is a healthy signal. This phenomenon will degrade the positioning performance of the GNSS technology. As a results, the performance of using 3D-GNSS in static data is not stable comparing to using it in dynamic data. It is essential to have another sensor to indicate the motion of pedestrian.

III. PEDESTRIAN DEAD RECKONING USING SMARTPHONE

This paper develops a smartphone based PDR system that consisted of two sensors and they are accelerometer and magnetometer. We do not use the gyroscope in the system because the proposed PDR is to put the smartphone in the pocket of trousers. The measurement of the gyroscope becomes very noisy in this setup. The proposed PDR first determines the orientation of device using the measured acceleration and magnetic field. At every measurement of the acceleration and magnetic field, the orientation of the device is estimated and the accelerometer readings are transformed into global coordinates. Afterwards, the step detection, stride estimation and heading orientation are applied subsequently. Steps are detected from the vertical acceleration sequence. At each step, the moving direction and the stride length of the user are estimated from the three components of acceleration. The position is then incremented from the previous step according to this direction and distance. It should be noted that the step detection component detects the steps of the left or right leg, depending on in which trouser pocket the device is located. This means that the stride length refers to the distance between two step points made by the same foot. The details of each algorithm are introduced as following.

A. Estimation of Device Orientation

The smartphone sensors output the 3-dimensional measurements in a local coordinate that defined by smartphones. The android operation system (OS) smartphone defines the X and Y axis are defined as left-to-right and bottom-to-top direction, respectively, of the display in portrait orientation. The Z axis is defined as the direction in which the display is facing. To make use of the measurements, the coordinate transformation to global coordinate is required. Android releases an open API called *getRotationMatrix* to provide the transformation. The idea of the transformation is to detect the gravity and then to match the three axes acceleration with it. Besides, the horizontal direction of the global coordinate is determined based on the reading of magnetometer, the detail of coordinate transformation can be found in Appendix. We apply a basic low-pass filtering of acceleration to attenuate the deterioration of dynamic pushes as shown below:

$$\hat{a}_i = \left(1 - \alpha^{acc}\right) a_i + \alpha^{acc} \left(\hat{a}_{i-1}\right), \tag{5}$$

$$\hat{e}_i = \left(1 - \alpha^{mag}\right) e_i + \alpha^{mag} \left(\hat{e}_{i-1}\right), \tag{6}$$

where, a and e denote the measured acceleration and magnetic field, respectively. The cap ^ indicates the filtered measurements. α denotes the smoothing factor, which is different with different smartphone. This research used a Google Nexus 5 to provide the measurements. We empirically set α^{acc} and α^{mag} as 0.6 and 0.84, respectively. With the help of the API, a rotation matrix is calculated, hence, the rotated measurement of the acceleration can be calculated.

B. Step Detection

During periodical walking motion, the sequence of vertical acceleration, a_V, displays one explicit peak and dip per
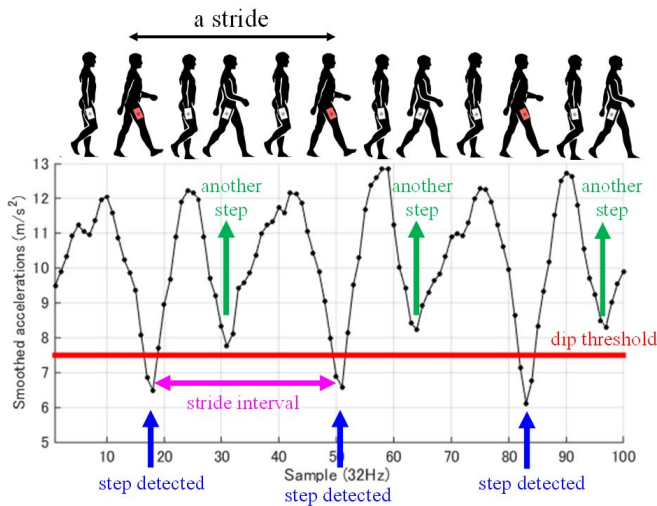
Fig. 5. Demonstration of the step detection using smoothed accelerations in vertical direction.

Fig. 6. Illustration of the verification of forward direction using forward acceleration.

one foot impact, irrespectively of how loosely the pocket is attached. After smoothing the sequence with a moving average to remove noise, we detect the dips of vertical acceleration as steps as shown in Fig. 5.

In this paper, the definition of stride is a distance of a cycle of walking motion, namely the distance travelled during a same leg to lift again. To avoid the false detection resulting from shallow dips (another step in Fig. 5), we set a dip threshold with 7.5 m/s^2 for our smartphone. Additionally, we also add a threshold of stride interval (pink in Fig. 5) to prevent the false detection of the shallow dips. The threshold is that the number of the accumulated samples between two step detections should be larger than one-third of samples in a second. Generally speaking, it is difficult to walk three steps in a second. The update rate of the smartphone used in this paper is 32 Hz. Therefore, the threshold of stride interval is 11 samples in this paper.

C. Estimation of Stride Length

Ideally, the stride of a pedestrian should be a constant. This is not always truthful in the real life. To derive the stride length, the peak-to-peak value of vertical acceleration a_V during each stride is used. A popular model to estimate the stride length is proposed by Weinberg [38] , and the model is shown as (7).

$$l = K_w \left(a_{V,max} - a_{V,min} \right)^{1/4}, \qquad (7)$$

where, K_w denotes a constant for unit conversion. In this paper, we empirically set K_w as 0.713 and 0.685 for male and female pedestrian, respectively.

D. Estimation of Heading Direction

This paper excludes the measurement of the MEMS gyroscope due to the smartphone is attached in the pocket of trouser. The variation of the tilt angle of the gyroscope becomes too large to use. Thus, we use the accelerations in
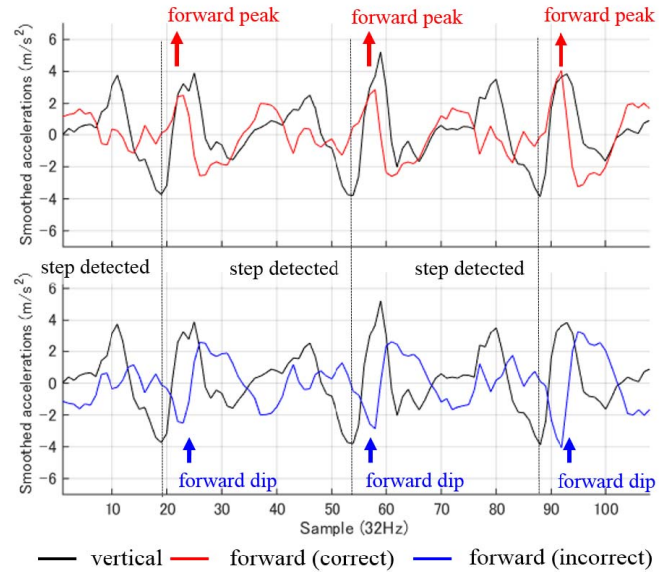
global coordinate to estimate the heading direction of pedestrian. Although, the heading error could be larger than the approaches using all sensors, we believe the pocket attachment is more practical than others.

In this paper, the heading direction is estimated in two steps. We first estimate the motion axis and then find its forward direction. The first step is based on principal component analysis (PCA) in 2-dimentional plane, following the method proposed in [21]. The back and forth movement of the leg produces a large variance of horizontal acceleration in a direction parallel to the motion axis. Therefore, PCA is applied in the sequence of east and north components of acceleration. Specifically, we first smooth the two sequences with a moving average, and then apply eigenvalue decomposition of the covariance matrix to them. The resulting first eigenvector gives an estimation of the direction that should be parallel to the motion axis. The length of the time window of PCA has to be longer than the walking cycle. We set 2 seconds in this paper. Although PCA method can estimate the motion axis, it is difficult to decide which direction of axis is the forward direction. To provide correct forward direction, we use the measurement forward acceleration. Note that the original forward direction acceleration is given by PCA method. To verify the original forward direction is correct or not, we check whether the forward acceleration has a peak or a dip after step detection as shown in Fig.6. The cyclic patterns of vertical and forward acceleration have a temporal relation [27]. The correct relation is a step detection is closely followed by a forward peak and vice versa as shown in Fig. 6.

E. Evaluation of Smartphone-Based PDR

In order to analyze the performance of the developed smartphone- based PDR, we test it with three male and a female objects in a general city environment. Each object repeats the same trajectory twice. We used a Google Nexus 5,

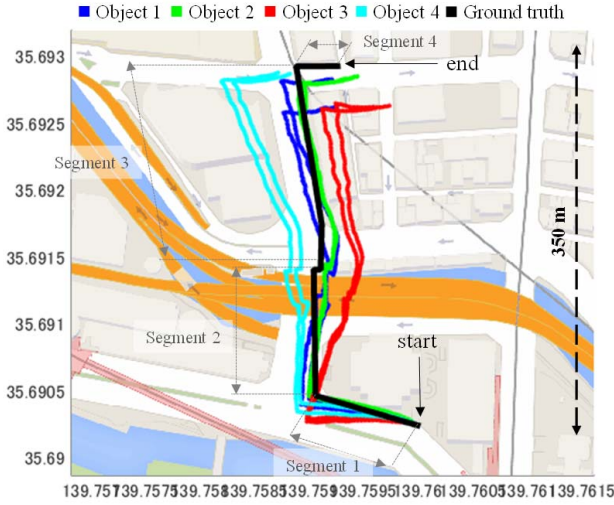| Sensor type	Model	Update rate
Accelerometer	MPU6515	32 Hz
Magnetometer	AK8963	32 Hz

Fig. 7. Positioning result of the smartphone-based PDR with 4 objects.

TABLE II

PERFORMANCE OF THE SMARTPHONE-BASED PDR SYSTEMS

Object	Heading error		Lateral positioning error	
	Mean	Std.	Mean	Std.
1	14.45°	15.33°	9.65 m	8.99 m
2	11.44°	17.78°	7.88 m	5.17 m
3	14.80°	16.51°	23.06 m	14.51 m
4	13.94°	17.17°	31.78 m	17.97 m

which is put in the pocket of trousers of the objects, to collect the measurements. Its specification of the sensors is listed in TABLE I.

The travelled distances of the walking tests are about 420 meters. Fig. 7 shows the walking trajectories estimated by the smartphone-based PDR. As shown in Fig. 7, the test trajectory is typical for general pedestrians. The shapes of the trajectories are very similar to the ground truth. The performance of Fig. 7 is listed in TABLE II.

The mean of heading error is less than 15 degrees in all the objects. With regards to the positioning error, the range is in between about 8 to 32 meters. The positioning error of objects 3 and 4 are larger than that of objects 1 and 2. After the Segment 1, as shown in the bottom of Fig. 7, the erroneous heading angle leads the accumulation of the positioning error in Segments 2, 3 and 4. Fig. 8 shows the lateral error of object 4 versus time. The error is accumulating over time. This phenomenon is common in PDR systems. Thus, it is important to integrate with other sensors or information aid to prevent the accumulating error. Note that the second trial of object 1 is a bit of shorter than another. It is because the 180° ambiguity in the PCA heading estimation method. This ambiguity will lead the estimation of PDR system to inverse direction.
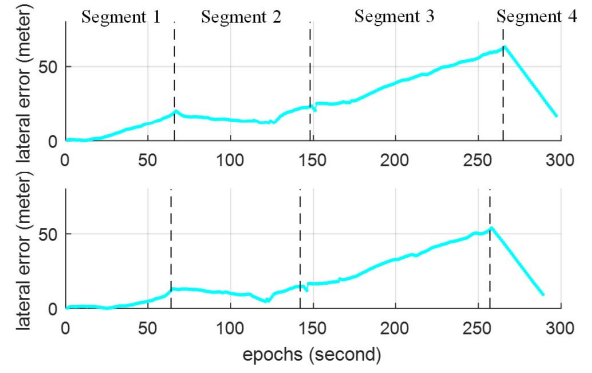

Fig. 8. Lateral error of the two test trials of object 4.
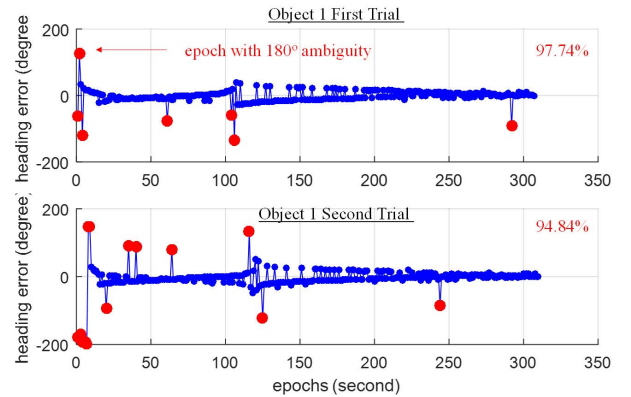

Fig. 9. Error of heading angle of the two test trials of object 1.

Fig. 9 demonstrates the heading error of tests of object 1. The red dot indicates the epoch with 180° ambiguity estimation. As shown in Fig. 9, the number of the epoch of the first trial is much less than that in the second trial. The correct estimation of the 180° ambiguity in the second test is about 95%, which is the worst in the eight trials. In overall, the developed smartphone PDR demonstrates not only its capability to provide continues solutions but also potential to indicate the pedestrian motions.

IV. INTEGRATION BASED ON KALMAN FILTER

This section introduces the algorithm of the developed Kalman filter, which integrated the 3D-GNSS and the smartphone-based PDR. The architecture of the integration system is shown in Fig. 10. Previously, both the 3D-GNSS and the PDR are introduced in Sections II and III, respectively. The algorithm of the implemented Kalman filter is detailed in the first subsection and the adaptive tuning algorithm of the Kalman filter is detailed in the second subsection. Note that if the smartphone supports to output GNSS pseudorange, the commercial GNSS receiver will be no longer required in the proposed system.

A. Total State Kalman Filtering

We implement a total state closed loop Kalman filter to estimate the position of pedestrian. The observed states are:

$$X_\mathbf{i} = \begin{bmatrix} x_i & y_i & \theta_i \end{bmatrix}^T \qquad (8)$$
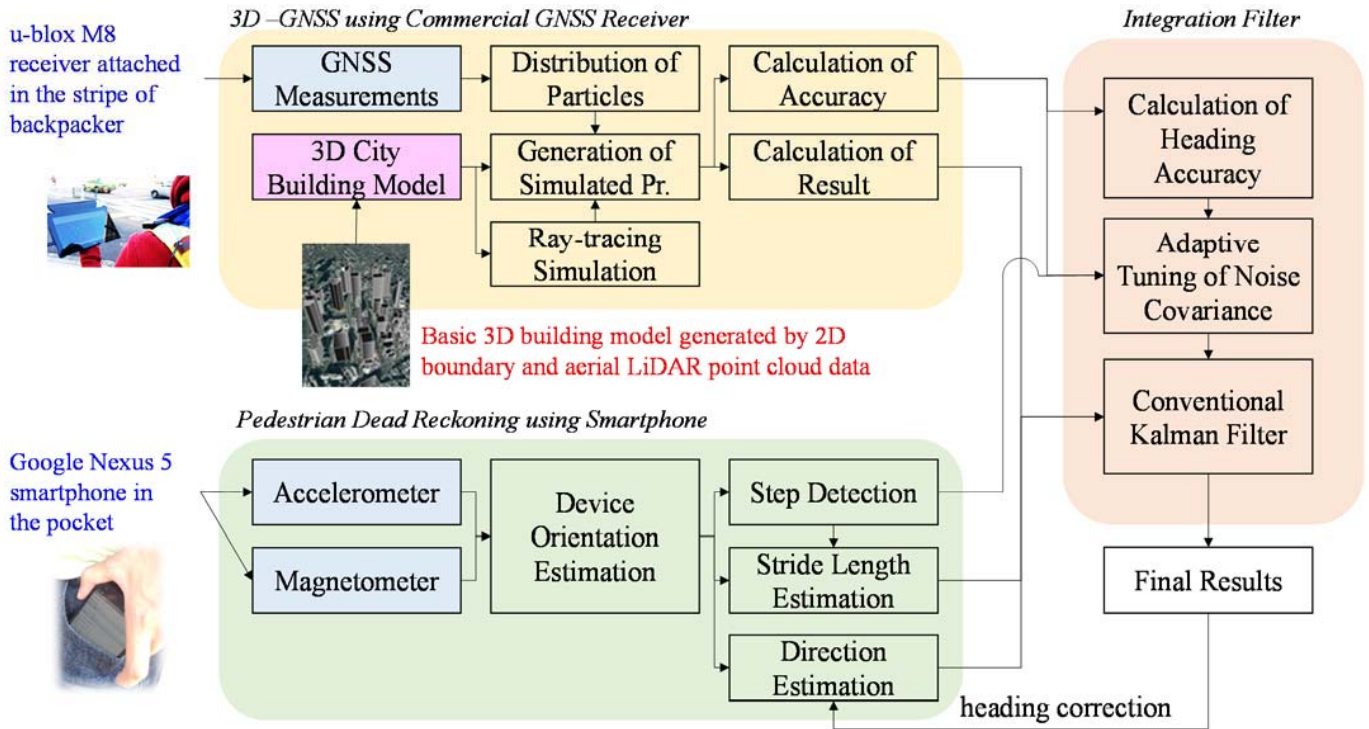
Fig. 10. Architecture of the proposed Kalman filter integration system. Both the flowchart of the proposed 3D-GNSS and smartphone-based PDR are included in the architecture.

where x_i, y_i, and θ_i denote the longitude, latitude and heading angle, respectively.

The 3D-GNSS provides the position and heading angle as measurements to the Kalman filter as shown below:

$$z = \begin{bmatrix} x_i^{3D-GNSS} & y_i^{3D-GNSS} & \Theta_i^{3D-GNSS} \end{bmatrix}^T \quad (9)$$

Thus, the observation matrix, H, is an identity matrix with rank 3. The proposed smartphone-based PDR provides the system input for the Kalman filter as shown in (10).

$$u_i = \begin{bmatrix} \frac{1}{rate} \cdot v \cdot cos\left(\theta_i^{PDR} - \delta\theta\right) \\ \frac{1}{rate} \cdot v \cdot sin\left(\theta_i^{PDR} - \delta\theta\right) \\ \theta_i^{PDR} - \delta\theta_i \end{bmatrix} \quad (10)$$

where $rate$ denotes the update rate of the Kalman filter, which is set as 1 Hz in this paper. v denotes the walking velocity obtain by the PDR. The walking velocity is calculated by the estimated stride dividing the time between two steps. $\delta\theta_i$ denotes the heading angle correction. It is calculated by the difference between the previous raw heading angle estimated by PDR and the previous updated heading angle by the Kalman filter as shown in (11).

$$\delta\theta_i = \theta_{i-1}^{PDR} - \theta_{i-1}^+ \quad (11)$$

where the superscript "+" denotes the updated state of the Kalman filter. By the use of the heading angle correction, the heading offset of PDR can be mitigated. Note that the PDR is not used as the propagation model because the walking trajectory of pedestrian tends to be nonlinear. Thus, we use a simple propagation model as (12). The propagation model used in this paper means prediction model.

$$F = \begin{bmatrix} 1 & 0 & 0 \\ 0 & 1 & 0 \\ 0 & 0 & 0 \end{bmatrix} \quad (12)$$

As can be seen from (12), the position remains the previous position if no step detected in the PDR system. With regards to the heading angle, the heading direction of pedestrian could change only within a few epochs. In the Kalman filter, the tuning of noise covariance is a key factor for its performance. The most common noise calibration method is to adjust the measurement noise covariance matrix (R), the propagation noise covariance matrix (Q) and the state estimation error covariance matrix (P) using empirical data. In general, the empirical tuning is to manually alter the value of P, Q, and R by the trial and error testing. One should note that the most crucial parameter of performance of Kalman filter is the ratio of the state error and measurement noise covariance matrices (P/R) [1]. If the setting of P/R is too small, the Kalman filter will converge in a slow fashion than it required. Conversely, if the P/R is overestimated, the Kalman filter would over believe the measurement noise which might result in a rapid diverge from the truth. In general, the state noise matrix is firstly set by predicting the error of state per epoch, then tuning the measurement noise matrix until the Kalman filter converged. With the respect of tuning the propagation noise matrix, it is based on the prediction of possible state error during the each estimation. It would be a challenge to change these noise covariance together due to that there are several undetermined parameters. In this research, we develop
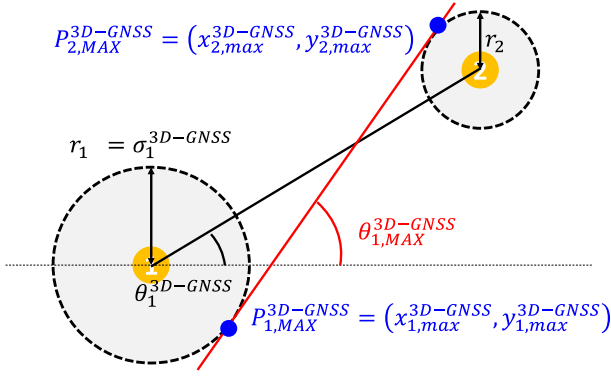
Fig. 11. Illustration of the calculation of the maximum heading error estimated by the 3D-GNSS.
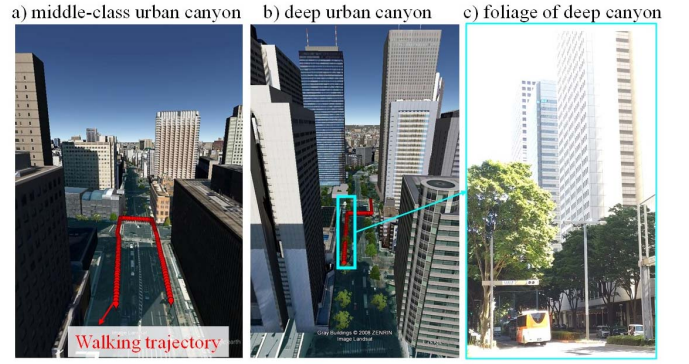

Fig. 12. Experiment environments. a) Middle-class urban canyon in Chiyoda area, Japan. b) Deep urban canyon in Shinjuku area, Japan. c) Foliage canyon by the street trees in the deep urban canyon. Courtesy: Google Earth.

an adaptive tuning method for the Kalman filter. The detail can be found in the next subsection.

B. Adaptive Tuning of Noise Covariance

The initial state noise matrix is set by a rough prediction of state's error per epoch. The measurement noise covariance matrix is updated adaptively. From Fig. 1, we can find there are two factors to affect the reliability of 3D-GNSS positioning method. They are the distribution of particles and the pseudorange similarity of the particles. The noise variance of the positioning performance of the 3D-GNSS can be calculated as (13).

$$\sigma^{3D-GNSS^2} = \left(\overline{d_{pr}^{(j)}}\right)^2 \times HDOP^{3D-GNSS}, \qquad (13)$$

where the superscript "–" denotes an average calculation and $HDOP^{3D-GNSS}$ denotes the horizontal dilution of precision (HDOP) of particles in the 3D-GNSS. The detail calculation of the $HDOP^{3D-GNSS}$ can be found in [7]. To calculate the possible maximum heading angle estimated by the 3D-GNSS, the previous calculated $\sigma_{3D-GNSS}^2$ is used. The idea is illustrated in Fig. 11.

According to Fig. 11, the maximum heading angle can be estimated by the blue points, $P_{i,MAX}^{3D-GNSS}$ as shown in (14). The $P_{i,MAX}^{3D-GNSS}$ However, the heading angle calculated by the 3D-GNSS is not consider only between two epochs. Follow the same idea in (4), the maximum heading error of 3D-GNSS is calculated in (15).

$$\theta_{i,MAX}^{3D-GNSS} = bearing\left(P_{i-1,MAX}^{3D-GNSS}, P_{i,MAX}^{3D-GNSS}\right), \qquad (14)$$

$$\Theta_{i,MAX}^{3D-GNSS} = \frac{\sum_{k=0}^{T-1}(T-k)\left(\theta_{i-k,MAX}^{3D-GNSS} - \theta_{i-k}^{3D-GNSS}\right)}{\sum_{k=0}^{T-1}(T-k)},$$
$$(15)$$

The off-diagonal terms of the adaptive R are assumed to be zero. This paper employs the variance of 3D-GNSS as the main diagonal terms of R, which shown in below:

$$R_i = \begin{bmatrix} K\sigma_i^{3D-GNSS^2} & 0 & 0 \\ 0 & K\sigma_i^{3D-GNSS^2} & 0 \\ 0 & 0 & \Theta_{i,MAX}^{3D-GNSS^2} \end{bmatrix} \qquad (16)$$

TABLE III
SPECIFICATION OF THE RECEIVERS USED

	Constellations	Update rate
Google Nexus 5	GPS/GLONASS/Beidou/SBAS	1 Hz
u-blox M8	GPS/GLONASS/QZSS/SBAS	1 Hz

where K denotes a constant factor, which is empirical set as 4 in this paper. The main sources of propagation noise are velocities and heading direction due to users' random motion. The propagation noise covariance matrix used is shown in (17).

$$Q = \begin{bmatrix} K^{PDR} & 0 & 0 \\ 0 & K^{PDR} & 0 \\ 0 & 0 & K^{\vartheta} \end{bmatrix} \qquad (17)$$

The developed smartphone based PDR can detect the motion of pedestrian step accurately. In the other words, it is capable of distinguishing the pedestrian motion in walking or standing. In the standing mode, the Kalman filter should rely on the PDR much more than 3D-GNSS because of the strong GNSS NLOS effects mentioned earlier. Thus, small K^{PDR} and K^{ϑ} are applied and they are 0.01, and $(1^o)^2$, respectively. In the walking mode, the K^{PDR} and K^{ϑ} are set empirically as 2 and $(15^o)^2$, respectively.

V. EXPERIMENTAL RESULTS AND DISCUSSIONS

A. Experiment Setup

The experiments are conducted in two typical urban areas, middle class and deep urban canyons as shown in Fig.12. The tests in this paper are performed at two sides of a street and a road intersection. There are two receivers used: u-blox EVK-M8 GNSS and Google Nexus 5. The acquirable constellation and update rate of the two receivers are listed in TABLE III.

The u-blox receiver and Google Nexus 5 are put in the strip of backpack and the pocket of trousers, respectively as shown in Fig. 10. There are five GNSS approaches, which is listed in TABLE IV, compared in this paper. The RTKLIB weighted least square (WLS) is a single point positioning method provided by open source RTKLIB software [39]. The satellites of the WLS approach uses line-of-sight (LOS) only is
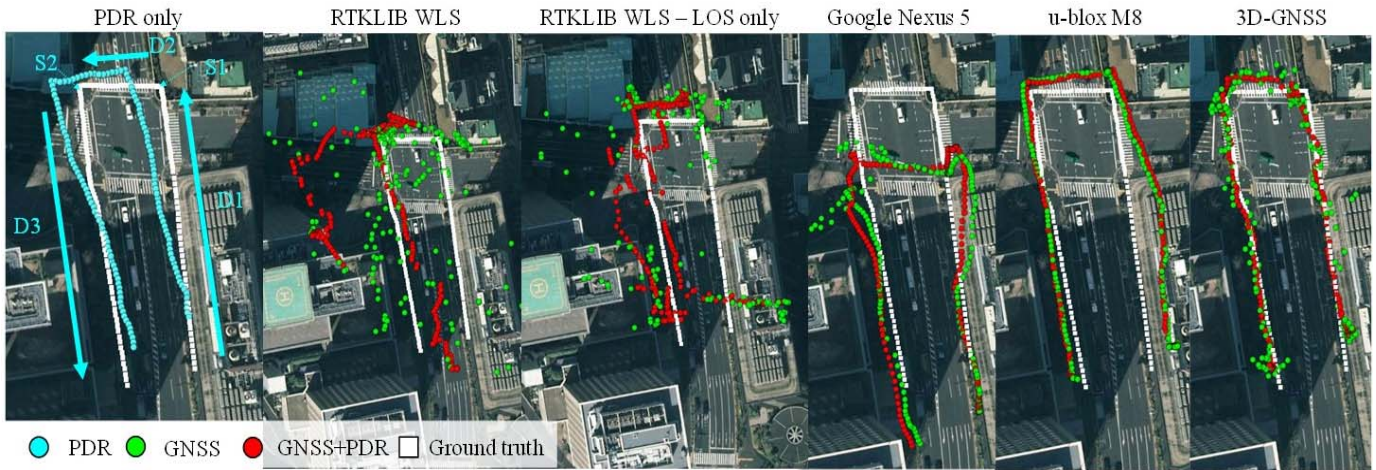
Fig. 13. Positioning results of different GNSS approaches and their integration results with the smartphone-based PDR in the middle-class urban canyon. Courtesy: Google Earth.

TABLE IV
DETAIL OF THE GNSS APPROACHES COMPARED

Approach	Receiver	Heading angle	Position
RTKLIB WLS	u-blox	Proposed Method	WLS
RTKLIB WLS (LOS only)	u-blox	Proposed Method	WLS
Google Nexus 5	Nexus	Receiver provided	Receiver
u-blox M8	u-blox	Proposed Method	Receiver
3D-GNSS	u-blox	Proposed Method	3D-GNSS

Fig. 14. Positioning error of the 3D-GNSS before (blue) and after (red) adding the smartphone-based PDR system in the middle-class urban canyon.

determined by the ray-tracing technique based on ground truth position. Note that this WLS LOS approaches only excludes the NLOS satellite, the multipath effect is still contained.

The quasi ground truth is generated using a topographical method. The video cameras are set in the 18th and 9th floors of a building near the Chiyoda and Shinjuku area, respectively, to record the travelled path. The video data output by the cameras are used in combination with one high-resolution aerial photo we bought to get the ground truth data. The aerial photo is 25cm/pixel and therefore the error distance for each estimate can be calculated. The performance metrics used are the mean and standard deviation of the lateral error and the availability. Availability means the percentage of solutions in a fix period. For example, if a method outputs 80 epochs in a 100 s period, the availability of the method is 80%.

B. Evaluation of the Integration System in Middle Urban Canyons

Fig. 13 and TABLE V show the positioning results of the five approaches standalone and their integration with the developed PDR system.

As can be seen from Fig. 13, the WLS approaches stand-alone provides very limited information about the walking trajectory pedestrian. The WLS using LOS only improves about 3 meters in the mean of positioning error but also loses about 26% of the availability. After integrating with the PDR system, their results become smoother. The standalone
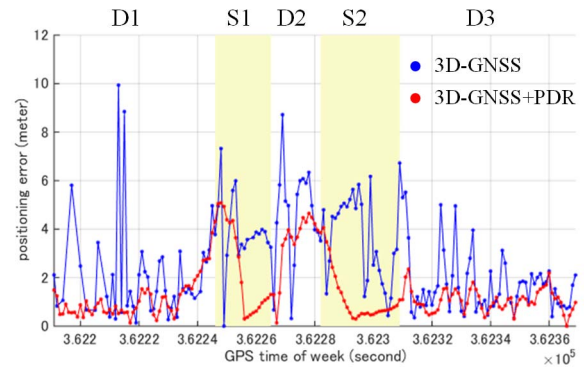
results of the commercial receivers, namely Google Nexus 5 and u-blox M8, can depict the shape of the walking trajectory. However, there is large shift in the Nexus solutions. For the u-blox receiver, it accurately estimates the position excepting in the D1 section (shown in the left of Fig. 13). Both commercial receivers are already smoothed using internal filter techniques, which are blinded to the users. As a result, they are not improved by the integration with the developed PDR system. With regarded to the proposed 3D-GNSS approach, its standalone results is very close to the ground truth. Its mean and standard deviation of positioning error are 2.65 and 1.98 meters, respectively. With the aiding of the smartphone-based PDR, its performance is further improved. Fig. 14 shows the positioning error of the 3D-GNSS before and after integrating with the PDR. In the most of the case, the large error of the 3D-GNSS can be mitigated by the PDR system. In addition, the error in the static periods, periods S1 and S2 in Fig. 14, is also greatly reduced. The reason of adding the PDR can reduce the positioning error is the use of the adaptive tuning mentioned in the previous chapter.

As shown in Fig. 15, the noise variance which calculated by (13) can reflect the positioning error of 3D-GNSS. Thus, it enables the Kalman filter to give appropriate weighting

TABLE V
PERFORMANCE OF DIFFERENT GNSS APPROACHES AND THEIR INTEGRATION RESULTS WITH THE
SMARTPHONE-BASED PDR IN THE MIDDLE-CLASS URBAN CANYON

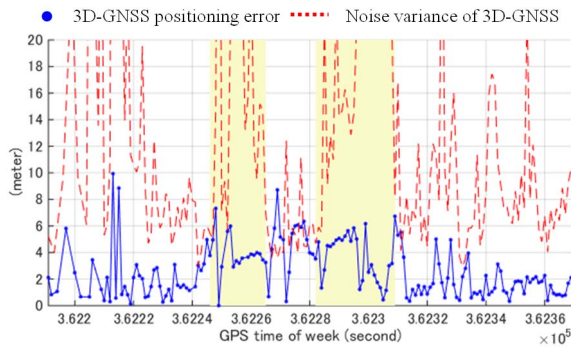|	RTKLIB WLS		RTKLIB WLS - LOS only		Google Nexus 5		u-blox M8		3D-GNSS	
	Standalone	Integration	Standalone	Integration	Standalone	Integration	Standalone	Integration	Standalone	Integration
Mean	15.62 m	21.82 m	12.77 m	12.65 m	12.06 m	10.71 m	4.33 m	4.40 m	2.65 m	1.45 m
Std.	24.39 m	24.24 m	12.96 m	9.50 m	9.67 m	8.02 m	2.34 m	2.41 m	1.98 m	1.22 m
Avail.	92.7%	100%	65.4%	100%	100%	100%	100%	100%	92.7%	100%

Fig. 15. Relationship between the positioning error of 3D-GNSS and its calculated noise variance.
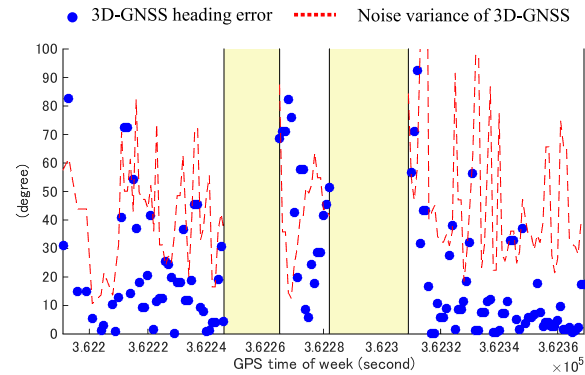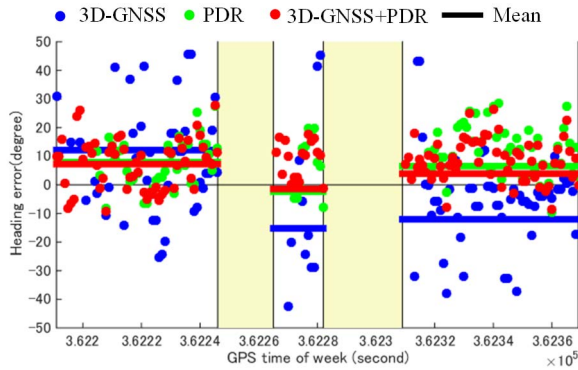

Fig. 16. Heading error of the 3D-GNSS, smartphone-based PDR and the integration system. The solid line indicates the mean value of the different approaches.

Fig. 17. Relationship between the heading error of 3D-GNSS and its calculated noise variance.

the heading angle estimated by the integrated system is smaller than that of the PDR standalone in three dynamic periods. This improvement reveals the heading error of the PDR can be reduced using the 3D-GNSS.

C. Evaluation of the Integration System in Deep Urban Canyons

The deep urban canyon selected in this paper not only surrounded by many skyscrapers but also contains street trees with dense foliage as shown in Figs. 12 (b) and (c). The street trees are only in the left side of the street. Thus, we conducted two kinds of experiments: 1) walking from relatively open area to the area with dense foliage and 2) walking from the area with dense foliage. First, we evaluate the first route. Figs. 18 and TABLE VI show the positioning results of the five approaches standalone and their integration with the PDR. The standalone results of the WLS approaches, again, cannot provide enough information to recognize the pedestrian trajectory in the D3 period, which is the area with dense foliage. Their availabilities are also lower than them in the middle-class urban canyon. By integrating with the PDR system, the walking trajectory can be derived. In the case of RTKLIB WLS, the WLS provide faulty position to the Kalman filter which miss-leads the integration results. In the case of WLS using LOS only, the approaches almost does not provide any solution in the D3 period. Therefore, its integration result follows the propagation of the PDR system. Both the commercial receivers perform good performance in the D1 and D2 periods. In the D3 period, both receivers are slowly diverged from the ground truth. With regards to the 3D-GNSS, its standalone performance is not as good as the

to 3D-GNSS. Importantly, the heading direction can be corrected using the 3D-GNSS. The heading direction of Periods D1, D2 and D3 are about 355, 270 and 85 degrees respectively. Fig. 16 shows the error of heading direction of the 3D-GNSS, the PDR and their integration. It can be seen that heading angles estimated by the 3D-GNSS, namely (4), are noisy in all three directions. If we use a constant value in the R of the Kalman filter, the estimated heading angle could be easily deteriorated by the 3D-GNSS. Hence, it is essential to calculate its maximum possible error to indicate the reliability of the 3D-GNSS estimated heading angle. As shown in Fig. 17, the noise variance which calculated by (15) can reflect the reliability of the estimated heading angle by the 3D-GNSS. Note that, it requires a few epochs to initialize the calculation of heading angle. Thus, the first few epochs after the static mode is not used in the integration. To observe Fig. 16,
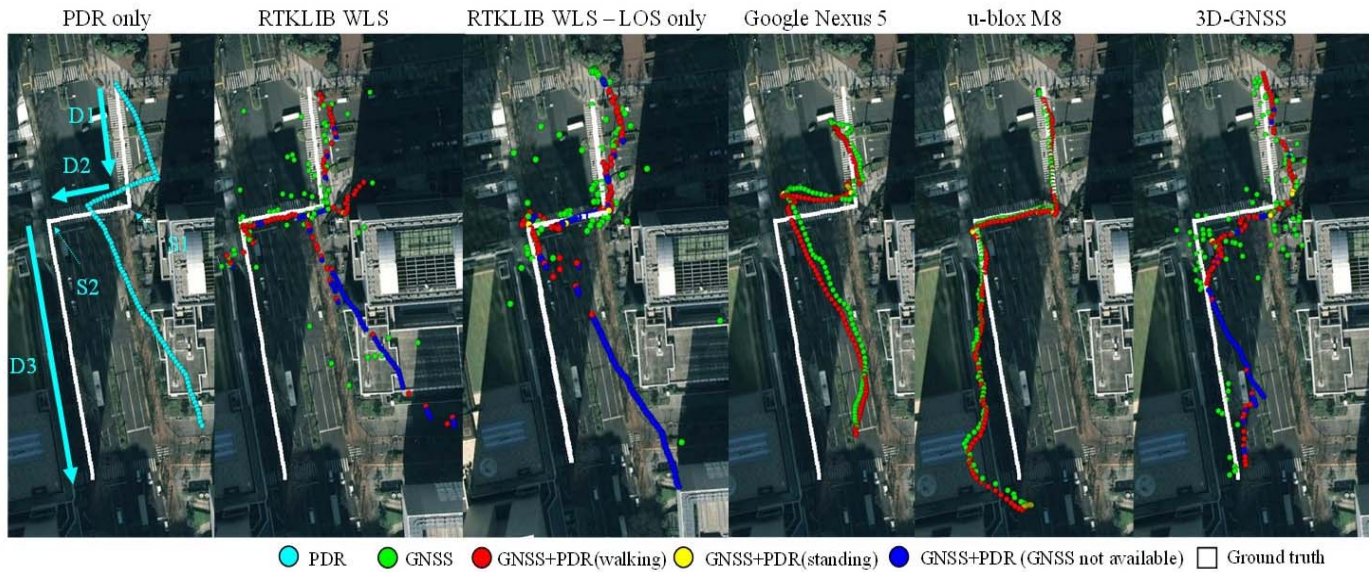
Fig. 18.   Positioning results of different GNSS approaches and their integration results with the smartphone-based PDR in the deep urban canyon. This experimental route is walked from relatively open area to the area with dense foliage. Courtesy: Google Earth.
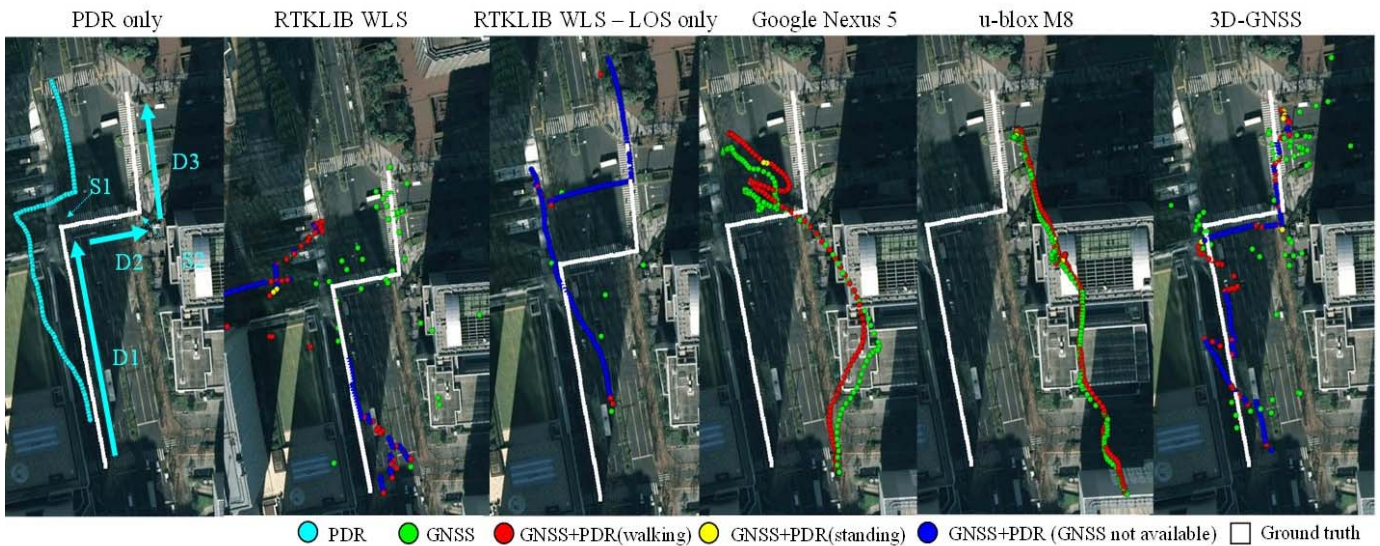

Fig. 19.   Positioning results of different GNSS approaches and their integration results with the smartphone-based PDR in the middle-class urban canyon. This experimental route is walked from the area with dense foliage to the relatively open area. Courtesy: Google Earth.

u-blox receiver in terms of the positioning error and availability. To compare their integrations with the PDR system, the u-blox receiver already applies a strong filter which results in its integration result is similar to its standalone performance. The adding of the PDR improves the 3D-GNSS greatly especially in terms of availability. To observe the right of Fig. 18, the integration obtain a better performance in the D3 period comparing to the u-blox integration result.

In the middle of the D3 period, the 3D-GNSS fails to provide solutions, hence its integration follows the propagation of the smartphone-based PDR. In the latter part of D3, the integrated system of 3D-GNSS and PDR can correct the pedestrian trajectory back to the vicinity of ground truth. Note that,

the 3D-GNSS approaches cannot correct the heading angle of the PDR in this deep urban test because of its low availability. Fig. 19 and TABLE VII show the positioning results of the second route in the deep urban canyon experiment. The main difference between the first and second routes is the GNSS performance in the beginning of the experiment. In the beginning of the second route, the GNSS performance is poor for all the approaches because of the insufficient number of received satellite. The commercial receivers usually require healthy GNSS signals to initialize their internal filter. Thus, the initial GNSS performance is essential to them. To observe the middle of Fig. 19, both commercial receivers fail to depict the pedestrian trajectory correctly. Fig. 20 shows the number

TABLE VI

PERFORMANCE OF DIFFERENT GNSS APPROACHES AND THEIR INTEGRATION RESULTS WITH THE SMARTPHONE-BASED PDR OF THE FIRST ROUTE IN THE DEEP URBAN CANYON

	RTKLIB WLS		RTKLIB WLS – LOS only		Google Nexus 5		u-blox M8		3D-GNSS	
	Standalone	Integration	Standalone	Integration	Standalone	Integration	Standalone	Integration	Standalone	Integration
Mean	15.27 m	19.03 m	10.78 m	14.29 m	12.08 m	11.02 m	4.03 m	4.32 m	6.25 m	5.63 m
Std.	22.65 m	18.69 m	17.47 m	14.05 m	7.70 m	7.28 m	4.80 m	4.57 m	5.51 m	2.89 m
Avail.	65.49%	100%	43.66%	100%	100%	100%	100%	100%	65.49%	100%

TABLE VII

PERFORMANCE OF DIFFERENT GNSS APPROACHES AND THEIR INTEGRATION RESULTS WITH THE SMARTPHONE-BASED PDR OF THE SECOND ROUTE IN THE DEEP URBAN CANYON

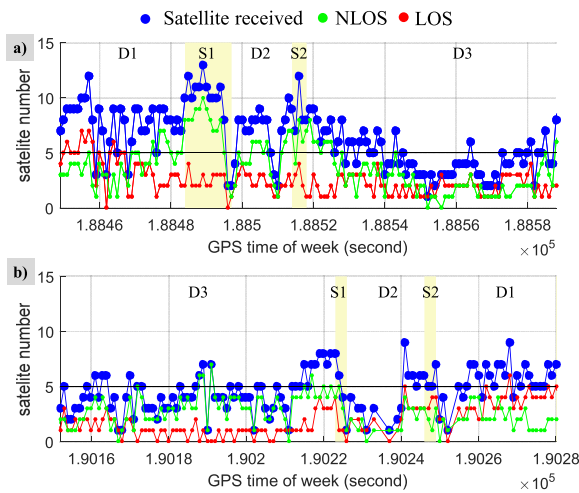|	RTKLIB WLS		RTKLIB WLS – LOS only		Google Nexus 5		u-blox M8		3D-GNSS	
	Standalone	Integration	Standalone	Integration	Standalone	Integration	Standalone	Integration	Standalone	Integration
Mean	21.93 m	35.96 m	18.11 m	24.96 m	26.20 m	25.21 m	39.30 m	39.79 m	10.43 m	4.30 m
Std.	27.85 m	25.88 m	9.49 m	4.65 m	12.07 m	10.44 m	19.21 m	19.08 m	8.55 m	2.36 m
Avail.	32.58%	100%	3.4%	100%	100%	100%	100%	100%	32.58%	100%

Fig. 20. Number of satellite received by the u-blox receiver. (a) and (b) denote the results for Figs. 18 and 19, respectively. The type of satellite is classified by ray-tracing technique based on ground truth.

of satellites received in the deep urban canyon experiments. Comparing Fig. 20 (a) and (b), the number of received satellite in the second test is much less than that in the first. As a result, the WLS approaches also have poorer performance than the previous experiment. The availabilities are only 32.6 and 3.4% for WLS and WLS using LOS only, respectively. There is only a few epochs that number of LOS is more than 5 in the second test. Thus, the integration result of the WLS using LOS only is almost done by the PDR propagation. The 3D-GNSS standalone also has worse performance comparing to the previous test, especially in the periods of D2 and D3. As shown in Fig. 20, the number of NLOS is more than the number of LOS in the periods. Although the standalone 3D-GNSS performance degrades, it is able to provide sufficiently accurate solutions in all the periods, namely D1, D2 and D3. Importantly, its integration with the PDR still has similar performance with the previous one. This reveals the proposed integrated system is able to estimate the pedestrian position accurately if 3D-GNSS can provide solutions.

VI. CONCLUSIONS

In this paper, a smartphone-based PDR system is developed. We studied the effectiveness of integrating PDR with different kind of GNSS approaches in urban canyon environments. In both middle and deep urban canyon environments, the conventional GNSS methods (WLS) are serious affected by multipath and NLOS effects. Integrating conventional GNSS method with PDR provides limited improvement of positioning accuracy. The performance commercial level GNSS receivers, such as GNSS receiver in Google Nexus 5 and u-blox M8, have better performance than the conventional GNSS methods. The reason is because these receivers already implemented filtering algorithms to smooth and/or select positioning results. However, because the positioning results of the commercial level GNSS receivers are the filtered and smoothed results. It is also difficult to evaluate the trustfulness of the positioning result in certain epoch. Therefore, the result of integrated system is close to the result of GNSS receiver. In middle and deep urbans, the performance of the integrated systems between commercial GNSS receivers and the developed PDR are satisfactory if the initialization of the systems are under healthy GNSS signals. In the case of the false initialization, the commercial receivers could totally get lost in deep urban canyon. The 3D-GNSS method could provide reliable performance in middle urban canyon. By integrating PDR with the 3D-GNSS method, we can achieve around 1.2 meters positioning mean error in such environment. In deep urban canyon, even though the performance of 3D-GNSS is not as good as it is in middle urban canyon, the 3D-GNSS method could identify trustful level of positioning results. In this case, integrating with PDR could improve the positioning mean error for more than 50%. Moreover, the availability of the 3D-GNSS could also be increased by integrating with PDR system.

APPENDIX
CALCULATION OF ROTATION MATRIX

To transfer the raw measurements from local (defined by smartphone) to global coordinate, a rotation matrix has

to be derived. The raw measurements from accelerometer and magnetometer can be expressed as vector form as (A.1) and (A.2), respectively:

$$|A| = \begin{bmatrix} a_x & a_y & a_z \end{bmatrix}^T \tag{A.1}$$

$$|E| = \begin{bmatrix} e_x & e_y & e_z \end{bmatrix}^T \tag{A.2}$$

First, we made an assumption that the accelerometer is mainly affected by gravity and the rests are negligible. Thus, the relationship between rotation matrix (C) and raw measurements from accelerometer is:

$$C \cdot A \cong \begin{bmatrix} 0 \\ 0 \\ |A| \end{bmatrix} \tag{A.3}$$

For the magnetometer, we also assume the magnetometer is mainly affected by geomagnetic field. We can obtain:

$$C \cdot E \cong \begin{bmatrix} 0 \\ |E| \sin \phi \\ |E| \cos \phi \end{bmatrix} \tag{A.4}$$

where ϕ denotes the angle between the magnetic line of force of geomagnetic field and the magnetometer. To define H as the cross product of vectors of acceleration and magnetic field:

$$H = (E \times A) = \begin{bmatrix} h_x & h_y & h_z \end{bmatrix}^T \tag{A.5}$$

$$\hat{H} = \begin{bmatrix} \frac{h_x}{|H|} & \frac{h_y}{|H|} & \frac{h_z}{|H|} \end{bmatrix}^T \tag{A.6}$$

where the cap $\hat{}$ denotes the normalization of the vector. To define M as the cross product of vectors of acceleration and vector H:

$$M = (A \times H) \tag{A.7}$$

Finally, we can obtain the rotation matrix C:

$$C = \begin{bmatrix} \hat{H}^T \\ \hat{M}^T \\ \hat{A}^T \end{bmatrix} \tag{A.8}$$

To verify (A.8), we calculate (A.3) by substituting (A.1) and (A.8):

$$C \cdot A = \begin{bmatrix} \hat{H}^T \cdot A \\ \left(\hat{A} \times \hat{M} \right)^T \cdot A \\ \hat{A}^T \cdot A \end{bmatrix} \cong \begin{bmatrix} 0 \\ 0 \\ |A| \end{bmatrix} \tag{A.9}$$

Note that vectors A, H and M are orthogonal to each other. Thus, their inner products are zero. Again, to verity (A.8), we call also calculate (A.4) by substituting (A.2) and (A.8):

$$R \cdot E = \begin{bmatrix} \left(\hat{E} \times \hat{A} \right)^T \cdot E \\ \left(\hat{A} \times \hat{E} \times \hat{A} \right)^T \cdot E \\ \hat{A}^T \cdot E \end{bmatrix} \cong \begin{bmatrix} 0 \\ |E| \sin \phi \\ |E| \cos \phi \end{bmatrix} \tag{A.10}$$

Thus, (A.8) is used as the rotation matrix.

REFERENCES

[1] P. D. Groves, *Principles of GNSS, Inertial, and Multi-Sensor Integrated Navigation Systems* (GNSS Technology and Applications), 2nd ed. Norwood, MA, USA: Artech House, 2013.

[2] P. Misra and P. Enge, *Global Positioning System: Signals, Measurements, and Performance*. Lincoln, MA, USA: Ganga-Jamuna Press, 2011.

[3] P. D. Groves, "Shadow matching: A new GNSS positioning technique for urban canyons," *J. Navigat.*, vol. 64, no. 3, pp. 417–430, 2011.

[4] M. Obst, S. Bauer, and G. Wanielik, "Urban multipath detection and mitigation with dynamic 3D maps for reliable land vehicle localization," in *Proc. IEEE/ION PLANS*, Myrtle Beach, SC, USA, Apr. 2012, pp. 685–691.

[5] T. Suzuki and N. Kubo, "GNSS positioning with multipath simulation using 3D surface model in urban canyon," in *Proc. ION GNSS*, Nashville, TN, USA, 2012, pp. 438–447.

[6] S. Peyraud *et al.*, "About non-line-of-sight satellite detection and exclusion in a 3D map-aided localization algorithm," *Sensors*, vol. 13, no. 1, pp. 829–847, 2013.

[7] L.-T. Hsu, Y. Gu, and S. Kamijo, "3D building model-based pedestrian positioning method using GPS/GLONASS/QZSS and its reliability calculation," *GPS Solutions*, to be published, doi: 10.1007/s10291-015-0451-7.

[8] S. Miura, L.-T. Hsu, F. Chen, and S. Kamijo, "GPS error correction with pseudorange evaluation using three-dimensional maps," *IEEE Trans. Intell. Transp. Syst.*, to be published, doi: 10.1109/TITS.2015.2432122.

[9] L. Wang, P. D. Groves, and M. K. Ziebart, "Smartphone shadow matching for better cross-street GNSS positioning in urban environments," *J. Navigat.*, vol. 68, no. 3, pp. 411–433, 2015.

[10] R. Kumar and M. G. Petovello, "A novel GNSS positioning technique for improved accuracy in urban canyon scenarios using 3D city model," in *Proc. 27th Int. Tech. Meeting Satellite Division Inst. Navigat. (ION GNSS)*, Tampa, FL, USA, 2014, pp. 2139–2148.

[11] A. Bourdeau, M. Sahmoudi, and J.-Y. Tourneret, "Constructive use of GNSS NLOS-multipath: Augmenting the navigation Kalman filter with a 3D model of the environment," in *Proc. 15th Int. Conf. Inf. Fusion (FUSION)*, Jul. 2012, pp. 2271–2276.

[12] L. T. Hsu, Y. Gu, and S. Kamijo, "NLOS correction/exclusion for GNSS measurement using RAIM and city building models," *Sensors*, vol. 15, no. 7, pp. 17329–17349, 2015.

[13] L. Fang *et al.*, "Design of a wireless assisted pedestrian dead reckoning system—The NavMote experience," *IEEE Trans. Instrum. Meas.*, vol. 54, no. 6, pp. 2342–2358, Dec. 2005.

[14] W. Chen, R. Chen, Y. Chen, H. Kuusniemi, and J. Wang, "An effective pedestrian dead reckoning algorithm using a unified heading error model," in *Proc. IEEE/ION Position Location Navigat. Symp. (PLANS)*, May 2010, pp. 340–347.

[15] S. Asano, Y. Wakuda, N. Koshizuka, and K. Sakamura, "A robust pedestrian dead-reckoning positioning based on pedestrian behavior and sensor validity," in *Proc. IEEE/ION Position Location Navigat. Symp. (PLANS)*, Apr. 2012, pp. 328–333.

[16] S. Beauregard, Widyawan, and M. Klepal, "Indoor PDR performance enhancement using minimal map information and particle filters," in *Proc. IEEE/ION Position Location Navigat. Symp. (PLANS)*, May 2008, pp. 141–147.

[17] A. R. Jimenez, F. Seco, C. Prieto, and J. Guevara, "A comparison of pedestrian dead-reckoning algorithms using a low-cost MEMS IMU," in *Proc. IEEE Int. Symp. Intell. Signal Process. (WISP)*, Aug. 2009, pp. 37–42.

[18] C. Huang, Z. Liao, and L. Zhao, "Synergism of INS and PDR in self-contained pedestrian tracking with a miniature sensor module," *IEEE Sensors J.*, vol. 10, no. 8, pp. 1349–1359, Aug. 2010.

[19] S. Beauregard, "A helmet-mounted pedestrian dead reckoning system," in *Proc. 3rd Int. Forum Appl. Wearable Comput. (IFAWC)*, Bremen, Germany, Mar. 2006, pp. 1–11.

[20] E. P. Herrera, R. Quirós, and H. Kaufmann, "Analysis of a Kalman approach for a pedestrian positioning system in indoor environments," in *Euro-Par 2007 Parallel Processing*, A.-M. Kermarrec, L. Bougé, and T. Priol, Eds. Berlin, Germany: Springer-Verlag, 2007, pp. 931–940.

[21] U. Steinhoff and B. Schiele, "Dead reckoning from the pocket—An experimental study," in *Proc. IEEE Int. Conf. Pervasive Comput. Commun. (PerCom)*, Mar./Apr. 2010, pp. 162–170.

[22] Y. Jin, H.-S. Toh, W.-S. Soh, and W.-C. Wong, "A robust dead-reckoning pedestrian tracking system with low cost sensors," in *Proc. IEEE Int. Conf. Pervasive Comput. Commun. (PerCom)*, Mar. 2011, pp. 222–230.

[23] H. Bao and W.-C. Wong, "Improved PCA based step direction estimation for dead-reckoning localization," in *Proc. Int. Conf. Cyber-Enabled Distrib. Comput. Knowl. Discovery (CyberC)*, Oct. 2013, pp. 325–331.

[24] N. Kakiuchi and S. Kamijo, "Pedestrian dead reckoning for mobile phones through walking and running mode recognition," in *Proc. 16th Int. IEEE Conf. Intell. Transp. Syst. (ITSC)*, Oct. 2013, pp. 261–267.

[25] J. Qian, L. Pei, J. Ma, R. Ying, and P. Liu, "Vector graph assisted pedestrian dead reckoning using an unconstrained smartphone," *Sensors*, vol. 15, no. 3, pp. 5032–5057, 2015.

[26] B. Shin, C. Kim, J. H. Kim, S. Lee, C. Kee, and T. Lee, "Hybrid model–based motion recognition for smartphone users," *ETRI J.*, vol. 36, no. 6, pp. 1016–1022, Dec. 2014.

[27] D. Kamisaka, S. Muramatsu, T. Iwamoto, and H. Yokoyama, "Design and implementation of pedestrian dead reckoning system on a mobile phone," *IEICE Trans. Inf. Syst.*, vol. E94-D, no. 6, pp. 1137–1146, 2011.

[28] D. Gusenbauer, C. Isert, and J. Krösche, "Self-contained indoor positioning on off-the-shelf mobile devices," in *Proc. Int. Conf. Indoor Positioning Indoor Navigat. (IPIN)*, Sep. 2010, pp. 1–9.

[29] F. Li, C. Zhao, G. Ding, J. Gong, C. Liu, and F. Zhao, "A reliable and accurate indoor localization method using phone inertial sensors," in *Proc. ACM Conf. Ubiquitous Comput.*, Pittsburgh, PA, USA, 2012, pp. 421–430.

[30] T. Akiyama, H. Ohashi, A. Sato, G. Nakahara, and K. Yamasaki, "Pedestrian dead reckoning using adaptive particle filter to human moving mode," in *Proc. Int. Conf. Indoor Positioning Indoor Navigat. (IPIN)*, Oct. 2013, pp. 1–7.

[31] W. Kang and Y. Han, "SmartPDR: Smartphone-based pedestrian dead reckoning for indoor localization," *IEEE Sensors J.*, vol. 15, no. 5, pp. 2906–2916, May 2015.

[32] H. Zhang, W. Yuan, Q. Shen, T. Li, and H. Chang, "A handheld inertial pedestrian navigation system with accurate step modes and device poses recognition," *IEEE Sensors J.*, vol. 15, no. 3, pp. 1421–1429, Mar. 2015.

[33] Y. Zhuang and N. El-Sheimy, "Tightly-coupled integration of WiFi and MEMS sensors on handheld devices for indoor pedestrian navigation," *IEEE Sensors J.*, to be published, doi: 10.1109/JSEN.2015.2477444.

[34] R. Harle, "A survey of indoor inertial positioning systems for pedestrians," *IEEE Commun. Surveys Tuts.*, vol. 15, no. 3, pp. 1281–1293, Jul. 2013.

[35] M. F. Iskander and Z. Yun, "Propagation prediction models for wireless communication systems," *IEEE Trans. Microw. Theory Techn.*, vol. 50, no. 3, pp. 662–673, Mar. 2002.

[36] P. D. Groves and Z. Jiang, "Height aiding, C/N_0 weighting and consistency checking for GNSS NLOS and multipath mitigation in urban areas," *J. Navigat.*, vol. 66, no. 5, pp. 653–669, 2013.

[37] M. S. Sharawi, D. M. Akos, and D. N. Aloi, "GPS C/N_0 estimation in the presence of interference and limited quantization levels," *IEEE Trans. Aerosp. Electron. Syst.*, vol. 43, no. 1, pp. 227–238, Jan. 2007.

[38] H. Weinberg, "Using the ADXL202 in pedometer and personal navigation applications," Analog Devices, Norwood, MA, USA, Tech. Rep. AN-602, 2002.

[39] T. Takasu and A. Yasuda, "Development of the low-cost RTK-GPS receiver with an open source program package RTKLIB," in *Proc. Int. Symp. GPS/GNSS*, Jeju, Korea, 2009, pp. 4–6.

Li-Ta Hsu (S'09–M'15) received the B.S. and Ph.D. degrees in aeronautics and astronautics from National Cheng Kung University, Tainan, Taiwan, in 2007 and 2013, respectively.

He was a Visiting Ph.D. Student with the Faculty of Engineering, University College London, London, U.K., in 2012. He is currently a Japan Society for the Promotion of Sciences Post-Doctoral Fellow with the Institute of Industrial Science, University of Tokyo, Tokyo, Japan. His research interests include all aspects of global navigation satellite system (GNSS) navigation, positioning, and signal processing, including wide-area differential GNSS systems and improving GNSS performance under challenging reception conditions, and indoor positioning techniques.
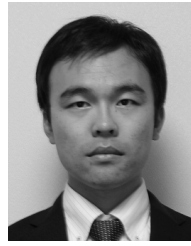
Yanlei Gu (M'14) received the M.E. degree from the Harbin University of Science and Technology, China, in 2008, and the Ph.D. degree from Nagoya University, Japan, in 2012. He has been a Post-Doctoral Researcher with the Institute of Industrial Science, University of Tokyo, since 2013. His research interests include computer vision, machine learning, and sensor integration for ITS.

Yuyang Huang received the B.E. degree from DongHuang University, China, in 2013. He is currently pursuing the master's degree in information and communication engineering with The University of Tokyo. His research topics are global navigation satellite system positioning and pedestrian dead-reckoning techniques.

Shunsuke Kamijo (M'97) received the B.S. and M.S. degrees in physics and the Ph.D. degree in information engineering from the University of Tokyo, Tokyo, Japan, in 1990, 1992, and 2001, respectively.

He was with Fujitsu Ltd., in 1992, as a Processor Design Engineer. Since 2001, he has been with the University of Tokyo, where he served as an Assistant Professor until 2002 and is currently an Associate Professor. His research interests include computer vision for traffic surveillance by infrastructure cameras and onboard cameras, cooperative systems using V2X communication, global navigation satellite system, and smartphone applications for ITS, and marketing. He is a member of the International Program Committee of the ITS World Congress, The Institute of Electronics, Information and Communication Engineers, the Society of Automotive Engineers of Japan, the Japan Society of Civil Engineers, and the International Association of Traffic and Safety Sciences. He is an Editorial Board Member of the *International Journal on ITS Research* (Springer) and *Multimedia Tools and Applications* (Springer).